Environmental Science & Technology

pubs.acs.org/est

Article

Unexpectedly Efficient Aging of Organic Aerosols Mediated by Autoxidation

Wen Zhang, Zixu Zhao, Chuanyang Shen, and Haofei Zhang*

Cite This: *Environ. Sci. Technol.* 2023, 57, 6965−6974

Read Online

ACCESS | Metrics & More | Article Recommendations | Supporting Information

ABSTRACT: Multiphase oxidative aging is a ubiquitous process for atmospheric organic aerosols (OA). But its kinetics was often found to be slow in previous laboratory studies where high hydroxyl radical concentrations ([•OH]) were used. In this study, we performed heterogeneous oxidation experiments of several model OA systems under varied aging timescales and gas-phase [•OH]. Our results suggest that OA heterogeneous oxidation may be 2−3 orders of magnitude faster when [•OH] is decreased from typical laboratory flow tube conditions to atmospheric levels. Direct laboratory mass spectrometry measurements coupled with kinetic simulations suggest that an intermolecular autoxidation mechanism mediated by particle-phase peroxy radicals greatly accelerates OA oxidation, with enhanced formation of organic hydroperoxides, alcohols, and fragmentation products. With autoxidation, we estimate that the OA oxidation timescale in the atmosphere may be from less than a day to several days. Thus, OA oxidative aging can have greater atmospheric impacts than previously expected. Furthermore, our findings reveal the nature of heterogeneous aerosol oxidation chemistry in the atmosphere and help improve the understanding and prediction of atmospheric OA aging and composition evolution.

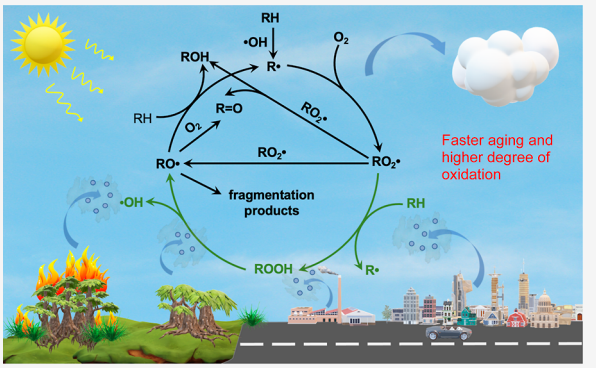

KEYWORDS: *heterogeneous oxidation, hydroxyl radicals, peroxy radicals, chain propagation, organic hydroperoxides*

INTRODUCTION

Organic aerosols (OA) are ubiquitously present in the Earth's atmosphere and greatly contribute to fine particulate matter.[1,2] The chemical composition and properties of atmospheric OA can significantly impact air quality, climate, and human health.[3,4] Despite the immense ubiquity of OA and the oxidizing nature of the atmosphere, the OA reactivity through heterogeneous oxidation by gaseous oxidants such as hydroxyl radicals (•OH) has often been considered a slow process[5−12] in comparison to the timescales of other important atmospheric processes and the overall aerosol lifetime.

The universal metric to quantify the heterogeneous oxidation kinetics is the effective reactive uptake coefficient of •OH (γ_{eff}), which describes the probability of •OH-particle collision leading to oxidation events[7]

$$\gamma_{eff} = \frac{4k\rho N_A V}{\bar{c} M A} \quad (1)$$

where k is the second-order degradation rate constant of an OA surrogate, ρ is the particle density, N_A is Avogadro's number, $\bar{c}$ is the mean thermal velocity of •OH, M is the molecular weight of the OA surrogate, V is the particle volume, and A is the particle surface area. Previous studies have often reported γ_{eff} in the range of 0.01−1.0,[5,8−11,13,14] with the smaller γ_{eff} values often observed for more viscous OA due to that oxidation is confined at the particle surface region which the inside materials cannot efficiently diffuse to. The kinetic information expressed in γ_{eff} could also allow for estimation of the OA oxidation timescales by[15]

$$\tau_{ox} = \frac{1}{k[^\bullet OH]} = \frac{2d_p\rho N_A}{3\gamma_{eff}\bar{c} M[^\bullet OH]} \quad (2)$$

where d_p is the particle diameter. Thus, the γ_{eff} value of 0.01−1.0 translates to oxidation timescales up to several years. These significantly longer timescales than the typical aerosol lifetime in the atmosphere (~10 days[16]) suggest that heterogeneous oxidation of OA in the atmosphere is less important in affecting air quality and the climate compared to some of the commonly focused processes such as secondary OA formation which usually has a timescale of only a few hours to a day. Furthermore, OA mass loss during heterogeneous oxidation within the relevant timescale was found to be minimal,

Received: December 27, 2022
Revised: April 6, 2023
Accepted: April 6, 2023
Published: April 21, 2023

https://doi.org/10.1021/acs.est.2c09773
Environ. Sci. Technol. 2023, 57, 6965−6974

suggesting that it is not an efficient aerosol removal process.[8] However, these long-standing views were derived from previous laboratory studies using •OH concentrations 3−5 orders of magnitude higher than atmospheric concentrations (i.e., [•OH] ∼ 10^9−10^{11} molecules cm^{-3}) to offset the short oxidation time (τ ∼ 1 min or less) in flow tube reactors (FTRs),[6,7,9−11,13,17] such that one can interpret OA oxidation under relevant atmospheric conditions, termed as "•OH exposure" (=[•OH] × τ).

Several prior studies have attempted to investigate the heterogeneous oxidation kinetics under lower [•OH] using FTRs,[15,18] continuous flow stirred tank reactors (CFSTRs),[19] or environmental chambers.[20] A summary of the scarce kinetic measurements from these studies (Figure S1) implies that lower [•OH] could enhance γ_{eff} to varied extents (greater enhancement for oxidized OA), but large uncertainties from distinct experimental conditions impede accurate interpretations. In most of these studies, such a [•OH]-dependent γ_{eff} was suggested to be caused by physical processes, including the following: (1) slower •OH reaction than the •OH adsorption at the gas−particle interface (i.e., the Langmuir−Hinshelwood mechanism),[15] (2) the diffusion limitation of organic molecules to the interface for •OH reaction,[20] or (3) O_3 (an •OH precursor) shielding the particle interface.[18] In contrast, Richards-Henderson et al. examined the chemical role of nitric oxide in increasing γ_{eff} via a chain propagation mechanism.[19] However, this mechanism is only relevant for highly polluted environment. It remains unclear whether [•OH]-dependent γ_{eff} may be explained by a generalized chemical mechanism relevant for typical atmospheric conditions.

Here, we probe the •OH-initiated heterogeneous oxidation of a few common OA model systems in a custom-designed CFSTR.[19,21−23] Experiments were conducted under a large range of [•OH] (5×10^6−1×10^9 molecules cm^{-3}) to bring the OA aging conditions from typical laboratory [•OH] closer to ambient levels. The chosen OA surrogates (adipic acid, succinic acid, citric acid, and 3-methylglutaric acid) are highly oxidized compounds (O/C ratio ∼0.7−1.2) containing multiple carboxylic acid functional groups. They all have been used in prior research to represent the oxygenated and viscous nature of generic OA in the atmosphere.[2,10,11,13,24−26] In these experiments, the particle diffusion coefficients (D_{org}, 10^{-8}−10^{-13} cm^2 s^{-1}) and mixing timescales (10^{-3}−10^2 s) are also representative of typical aerosol phase states in the lower troposphere.[26] Their degradation upon heterogeneous •OH-oxidation was monitored in real-time using a thermal desorption iodide-adduct chemical ionization mass spectrometer (TD-CIMS) to provide accurate kinetic measurements.[27,28] The comprehensive OA oxidation products were measured by the TD-CIMS and an ion mobility spectrometry time-of-flight mass spectrometer (IMS-MS)[24,27,29−31] which provides additional isomer-resolved capability. Complementary FTR experiments were also performed following similar procedures as in previous studies.[27,30] This allows for direct comparisons of the heterogeneous oxidation kinetics and products between the CFSTR and FTR experiments. In addition, a multilayer reaction-diffusion kinetic model was developed to simulate and interpret the experimental results.[27]

MATERIALS AND METHODS

Experimental Setup. All experiments were performed at 22 °C and varied water activity (a_w of 35−70%). A customized CFSTR (volume ∼250 L)[31,32] was used in this work with the setup shown in Figure S2. Here, the CFSTR was operated in the "semibatch" mode under room temperature.[21] Before each experiment, the CFSTR was flushed overnight with clean dry air, supplied by a zero-air generator (AADCO Instrument, Inc.). At the beginning of each experiment, the CFSTR background was monitored to ensure that aerosol particles were not present. Polydisperse organic aerosols (OA) of selected model compounds were generated into the CFSTR using a constant output aerosol atomizer (TSI, Inc.). The OA injection was stopped when targeted OA mass concentration was reached (∼2000−3000 μg m^{-3}). The high OA mass loading is necessary to allow sufficient detection of OA composition by several techniques and eliminate evaporation of parent OA during experiments. After OA injection, the clean air injection was adjusted to a total flow of 1.5 L min^{-1}. Two different a_w levels were studied for the OA model compounds: 0.36 ± 0.01 and 0.67 ± 0.03. For adipic acid and succinic acid, the injected OA through the dryer effloresced the particles and a_w levels do not change their phase state and D_{org}. However, for citric acid that does not have an efflorescence point, different a_w levels lead to different amounts of water in the OA and hence affect the phase state and D_{org}.[11,33,34] The 3-methylglutaric acid OA was only studied under a_w = 0.36. In all the CFSTR experiments, the mean surface-weighted particle diameters for adipic acid, succinic acid, citric acid, and 3-methylglutaric acid were 210 ± 50 nm, 420 ± 120 nm, 290 ± 15 nm, and 221 ± 17 nm, respectively. After the OA injection, a one-time injection of a VOC tracer (either acetic acid or propionic acid) was made to reach a VOC concentration of 1−2 ppm. After both the OA and VOC tracer have been injected, they were allowed to undergo dilution (caused by the continuous flow) and wall loss in the CFSTR (Figure S3). Then, either O_3 or H_2O_2 was continuously injected into the CFSTR. With the mercury UV lamps on (λ = 254 nm), this injection initiated the in situ generation of •OH radicals.[27,30] By changing the injection concentration of O_3 or H_2O_2, the [•OH] was controlled. During the •OH-initiated oxidation, the total flow rate and a_w were maintained the same as the "dilution and wall loss only" period. Therefore, the changes in the decay rates of both the OA and VOC tracer were caused by oxidation. The oxidation was maintained for 1−2 h. To compare results obtained from the CFSTR experiments, auxiliary FTR experiments were performed in parallel with the CFSTR studies. The setup for the FTR is the same as our previous work.[24,27,29,30] The injection system and the kinetic measurements are the same as for the CFSTR experiments. In both reactors, NO_x is below our detection limit (<0.5 ppb) and is expected to play a negligible role in the OA aging experiments.

Instrumentation. The schematics of the instrumentation are shown in Figure S2. The OA particle size distribution and number concentration were analyzed by a scanning electrical mobility spectrometer and mixing condensation particle counter (SEMS and MCPC, Brechtel Inc.). A high-sensitivity proton-transfer-reaction mass spectrometer (PTR-MS, IONICON Analytik Inc.) was used to measure the decay of the VOC tracers at 0.3 L min^{-1} in some experiments.[35] The OA composition was measured in real time by an iodide-adduct time-of-flight CIMS (Aerodyne Research Inc., $m/\Delta m$ ∼ 4000) with a TD tube following a charcoal denuder to remove volatile gases.[27,28,31] The desorption temperature was set to 90−160 °C for different OA systems to vaporize most of the particle mass (>90%) and almost all the parent OA species.

https://doi.org/10.1021/acs.est.2c09773
Environ. Sci. Technol. 2023, 57, 6965−6974

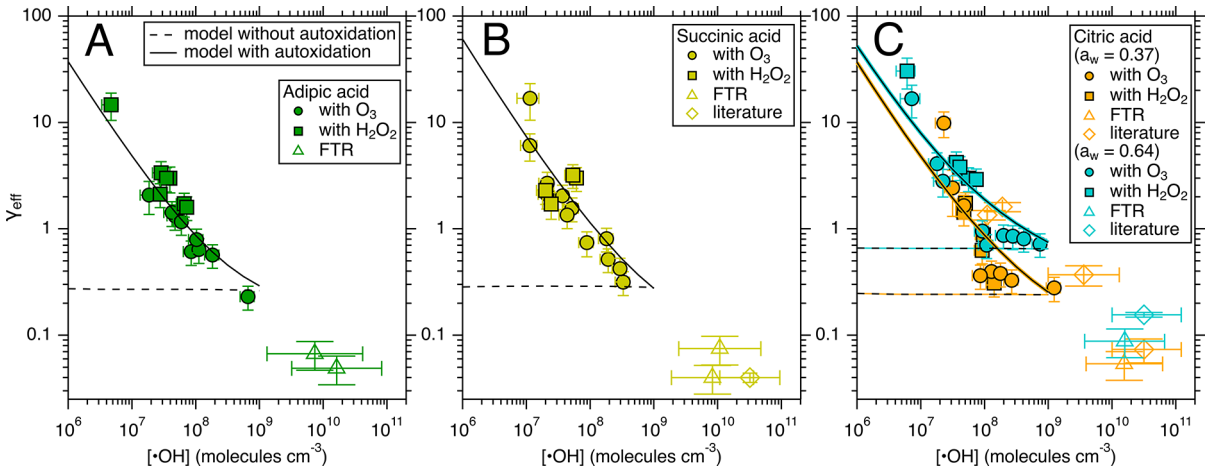

Figure 1. γ_{eff}–[•OH] relationship for OA surrogate systems. (A) Adipic acid, (B) succinic acid, and (C) citric acid, under various experimental conditions (see figure legend). For succinic acid (B) and citric acid (C), measurements from a few prior studies are also shown.[10,11,13,20] For citric acid, experiments were performed under two different a_w conditions, resulting in different D_{org} values (see the Supporting Information). Model simulations with and without the consideration of autoxidation are shown with the experimental data. Similar γ_{eff}–[•OH] trend obtained from three 3-methylglutaric acid experiments (Figure S5) is in general consistency with the results shown here.

For the experiments in which the PTR-MS was unavailable, the VOC tracers were also monitored by the CIMS, where a separate gas sampling line was added bypassing the TD unit. The oxidation of 3-methylglutaric acid and adipic acid OA was used as the model system for the offline chemical composition analysis and comparison between the CFSTR and FTR results. The oxidized OA particles were collected using a sequential spot sampler (Aerosol Devices Inc.) downstream of a charcoal denuder. The collected OA samples were immediately extracted by acetonitrile and infused into an electrospray ionization (ESI) IMS-MS (Aerodyne Research Inc.) in the negative ion mode. The IMS-MS measurements could provide isomer-resolved characterization by separating ionized molecules with their structure-dependent collisional cross sections.[36,37] More details were described in our prior studies.[24,27,30,32] Finally, a UV–visible spectrophotometer (Agilent Inc., 8453) was used for total ROOH quantification (see the Supporting Information for details).

Calculations of the Heterogeneous Oxidation Kinetics and Timescales. By comparing the decay rates of the parent OA compound and the VOC tracer before and after the oxidation (Figure S3), the [•OH] in the CFSTR and the second-order oxidation rate constants (k) of parent OA compound through heterogenous OH oxidation were determined. Specifically, the •OH oxidation rate constants of acetic acid and propionic acid ($k_{VOC+•OH}$) were known from the literature (6.6×10^{-13} cm^3 molecule^{-1} s^{-1} and 1.64×10^{-12} cm^3 molecule^{-1} s^{-1}, respectively).[38,39] Thus, the [•OH] can be calculated by

$$[^{\bullet}OH] = \frac{k_{VOC,ox} - k_{VOC,DL}}{k_{VOC+\cdot OH}} \quad (3)$$

where $k_{VOC,ox}$ and $k_{VOC,DL}$ are the first-order VOC decay rates during the oxidation period and the dilution-wall loss period, respectively. Then, the second-order oxidation rate constants (k) of parent OA compound through heterogenous •OH oxidation was calculated by

$$k = \frac{k_{OA,ox} - k_{OA,DL}}{[^{\bullet}OH]} \quad (4)$$

where $k_{OA,ox}$ and $k_{OA,DL}$ are the first-order parent OA decay rates during the oxidation period and the dilution-wall loss period, respectively. The four first-order decay rates ($k_{VOC,ox}$, $k_{VOC,DL}$, $k_{OA,ox}$, and $k_{OA,DL}$) were obtained from the PTR-MS or TD-CIMS measurements. The high-frequency measurements made by the two instruments allow for high confidence decay rates, and hence reliable estimates of k. The k values were then used to calculate the effective uptake coefficient (γ_{eff}) shown in eq 1.[7] Therefore, the relationships between the γ_{eff} and [•OH] can be obtained. The oxidation timescales are hence estimated by eq 2.[15]

The Reaction-Diffusion Multilayer Kinetic Model. To explain the experimental observation, a reaction-diffusion multilayer kinetic model was developed, as described in our previous work[27] and is essentially a similar representation to several other models that simulates heterogeneous OA oxidation processes.[40−42] The model constructs a multi-compartment rectangular prism to approximate the OA particle (Figure S4). The area of the square surface of the prism is set to be the same as the spherical OA aerosol in the experiments, and the height of the rectangular prism is $d_p/6$ to maintain the same surface-to-volume ratio of the spherical aerosol and hence preserves the relevant scaling between surface and bulk processes. The thickness of each compartment is set to 0.5 nm, which was suggested to be a good representation of semisolid and solid aerosol particles.[42] Each compartment is assumed to be a well-mixed volume. The model includes (1) the adsorption, desorption, and reactions of •OH and HO_2• at the outermost (i.e., surface) compartment of the OA particles, (2) organic radical-centered and multi-generational reactions in each compartment, and (3) diffusions of all the species molecules between compartments and evaporation of the relatively volatile products from the surface compartment to gas phase. The FACSIMILE software was used to perform the simulations.[27] See the Supporting Information for more details.

RESULTS AND DISCUSSION

Heterogeneous Oxidation Kinetics. As shown in Figure 1, the measured γ_{eff} exhibits striking enhancement as [•OH] decreases from ~1×10^9 to ~5×10^6 molecules cm^{-3} for all

https://doi.org/10.1021/acs.est.2c09773
Environ. Sci. Technol. 2023, 57, 6965−6974

the studied OA systems. As [•OH] approaches atmospheric levels (10^6–10^7 molecules cm^{-3}), the γ_{eff} values are 2–3 orders of magnitude higher than those obtained from the high-[•OH] FTR experiments performed in this work and in prior studies. It is also worth noting that in the citric acid system, where varied a_w was studied, higher a_w and hence faster diffusion in the particles led to larger γ_{eff} under [•OH] > ~ 10^8 molecules cm^{-3} (Figure 1C), agreeing with prior work.[11,13,43] However, the difference appears to diminish as [•OH] further drops, implying that particle-phase diffusion may not be a key limitation for OA multiphase oxidative aging under ambient conditions. These kinetic results suggest that OA heterogeneous oxidation in the atmosphere may have a much shorter timescale than previously expected. For example, for a 500 nm diameter particle under [•OH] of 10^6 molecules cm^{-3}, γ_{eff} of 10 indicates an oxidation timescale of ~2.3 days, compared to 231 days when γ_{eff} is 0.1. These kinetic results are qualitatively consistent with prior studies (Figure S1), but contain more data points with smaller uncertainties, and hence are directly comparable to obtain the [•OH]-dependent γ_{eff}.

To investigate the cause of the [•OH]-dependent γ_{eff}, we used a multilayer reaction-diffusion kinetic model (see the Supporting Information for details). The model explicitly considers the adsorption and desorption of •OH at the gas–particle interface and the diffusion and reactions at the particle surface and in the bulk.[27,40,44] The main reaction mechanism in the model is shown in Figure 2 (top part), where self-reaction

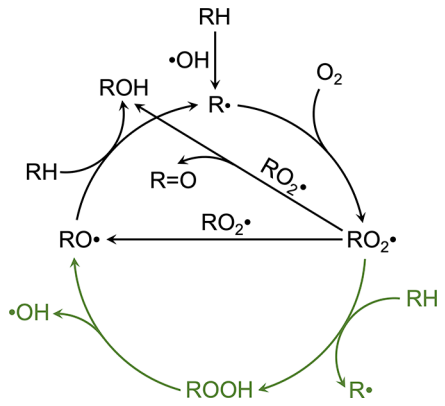

Figure 2. The •OH-initiated heterogeneous oxidation mechanism of organic aerosols in the atmosphere. The top part of the scheme (in black) illustrates the previous mechanistic understanding, and the bottom part (in green) shows the autoxidation mechanism proposed in this work.

of peroxy radical ($RO_2^•$) plays a central role: •OH oxidizes a parent OA molecule (RH) through H-abstraction and produces an alkyl radical (R•); $RO_2^•$ is subsequently formed following oxygen addition; the $RO_2^•$ + $RO_2^•$ self-reaction then produces an alcohol–carbonyl pair (ROH and R=O), known as the Russell mechanism, or two alkoxy radicals ($RO^•$);[5,45] the $RO^•$ may decompose to smaller oxidized products or undergo chain propagation reactions (i.e., $RO^•$ + RH),[19] forming an alcohol product and a new $RO_2^•$. The mechanism may occur at multiple generations, forming multifunctional products.[7,24] For instance, both ROH and R=O can be further oxidized to form $R(OH)_2$ (diol), $R(=O)_2$ (dicarbonyl), and R(=O)OH (hydroxycarbonyl). This mechanism has been widely accepted to explain the major heterogeneous OA oxidation products observed in prior research. However, the kinetic model with this mechanism fails to simulate the increased γ_{eff} with reduced [•OH] (Figure 1), indicating that the traditional $RO_2^•$ + $RO_2^•$ dominant chemistry cannot explain the observations. Moreover, the results also suggest that the previously attributed Langmuir–Hinshelwood mechanism[15] and particle-phase diffusion limitation[20] do not explain the increased γ_{eff} with reduced [•OH] under the studied conditions of [•OH] and particle D_{org} because these processes are already implemented in the kinetic model. The model performance is consistent with other models developed in previous studies which also considered these processes.[14,44] The O_3 shielding mechanism[18] can also be ruled out as we observed similar γ_{eff}–[•OH] behavior by using H_2O_2 as the •OH precursor instead of O_3 (Figure 1). Furthermore, the previously proposed $RO^•$-driven chain propagation reactions could only slightly enhance γ_{eff},[19] and is independent of [•OH] (Figure S6). Therefore, the [•OH]-dependent γ_{eff} suggests that a previously unrecognized mechanism is needed to explain the high γ_{eff} under low [•OH].

Oxidation Products Highlight the Formation of Organic Hydroperoxides. To elucidate the unrecognized mechanism, we further examined the oxidation products (Figure 3). Consistent with the above-mentioned reaction scheme, the most abundant products observed from these experiments by the TD-CIMS are R=O and ROH from the $RO_2^•$ + $RO_2^•$ self-reaction. Interestingly, another major product with two additional oxygens than RH ("RH + 2O") was also observed in some of the studied OA systems. We determine this product to be the organic hydroperoxide (ROOH) for the reasons discussed below. Although the same chemical formula could be the second-generation products $R(OH)_2$, the absence of the other two expected concurrent second-generation products [i.e., R(=O)OH and $R(=O)_2$] from the TD-CIMS measurements ruled this out (Figure 3A,B). In contrast, these expected second-generation products were all observed in the high-[•OH] FTR experiments. Additionally, the "RH + 2O" signal appears almost simultaneously with the onset of •OH oxidation, while a second-generation product is usually indicated by delayed formation.[7] To further confirm its identity, the IMS-MS was used to compare the oxidation products between experiments under different [•OH] on the isomer-resolved level and with higher sensitivity. In this comparison (Figure 4), adipic acid oxidation under very different [•OH] produced identical isomer distributions and abundances for both R=O and ROH (Figure 4A,B,D,E). In contrast, "RH + 2O" exhibits very different isomer distributions between the two [•OH] conditions, with a unique and dominant isomer present only under lower [•OH] (Figure 4 C vs F), providing unambiguous evidence for ROOH formation. Moreover, auxiliary total hydroperoxide analysis also supports the formation of ROOH under low [•OH] in the CFSTR (Figure S7). In Figure 3C,D, we present the signal-based fractions of R=O and "RH + 2O" among the three major products as a function of [•OH] in the adipic acid system, where all three products were detected. The results, compared with measurements from the high-[•OH] FTR experiments, clearly show that the formation of R=O is inhibited, while "RH + 2O" (mostly ROOH) is enhanced under low [•OH]. On the contrary, most of "RH + 2O" detected under high [•OH] in the FTR are $R(OH)_2$ (Figure 4F). This [•OH]-dependent OA composition also explains the contradiction between this work and prior studies which reported no evidence of ROOH formation,[7,46] as prior studies used high [•OH] to investigate OA oxidative aging. Finally, to

https://doi.org/10.1021/acs.est.2c09773
Environ. Sci. Technol. 2023, 57, 6965–6974

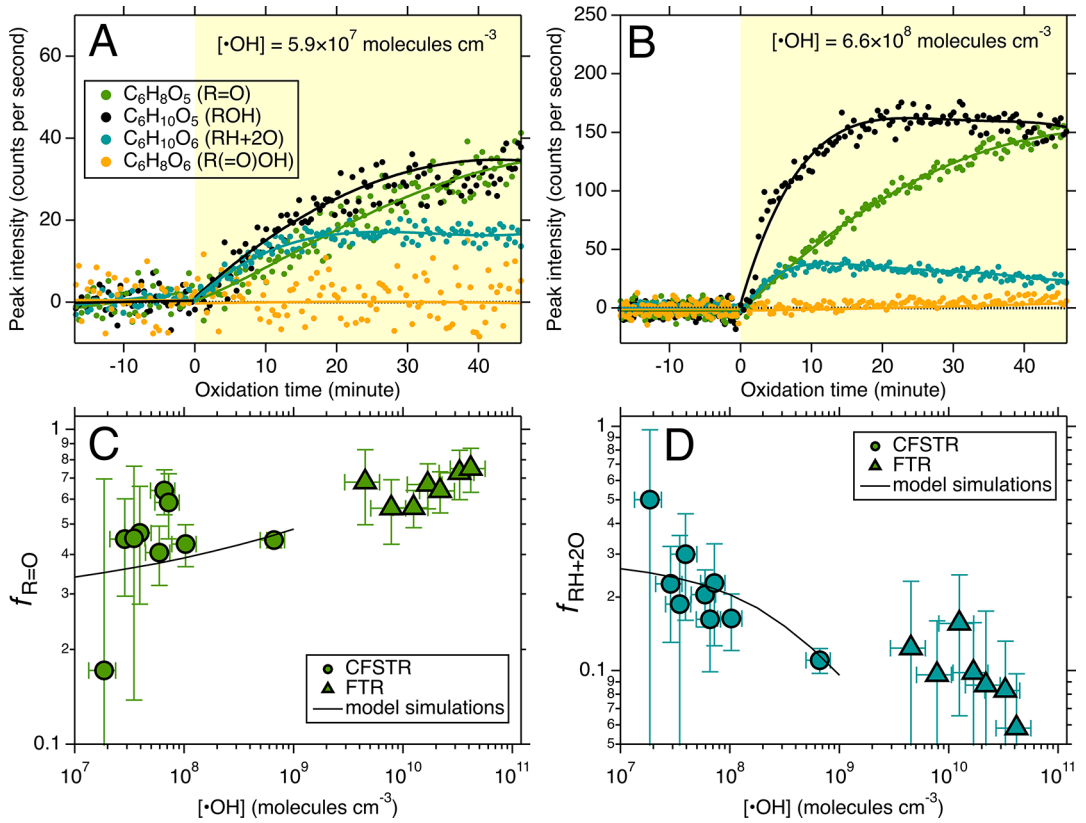

Figure 3. Major products from adipic acid OA oxidation. (A,B) TD-CIMS time-series of the three major first-generation products (i.e., R═O, ROH, and "RH + 2O") for two adipic acids oxidation CFSTR experiments under different [•OH]. For comparison, one of the second-generation products [R(═O)OH] is shown. The other second-generation product, $R(=O)_2$, is also absent as R(═O)OH and hence is not shown. The light-yellow shades suggest the oxidation periods; the fitted curves are to guide the eye. (C,D) The fractions of R═O and "RH + 2O" in the first-generation products from adipic acid oxidation experiments. The error bars represent the measurement standard deviation, and the curves are model results. The model simulations with autooxidation only considers the ROOH as $R(OH)_2$ is not explicitly represented in the model. The simulations show consistent trends with the measurements. The similar time series results for 3-methylglutaric acid are shown in Figure S8.

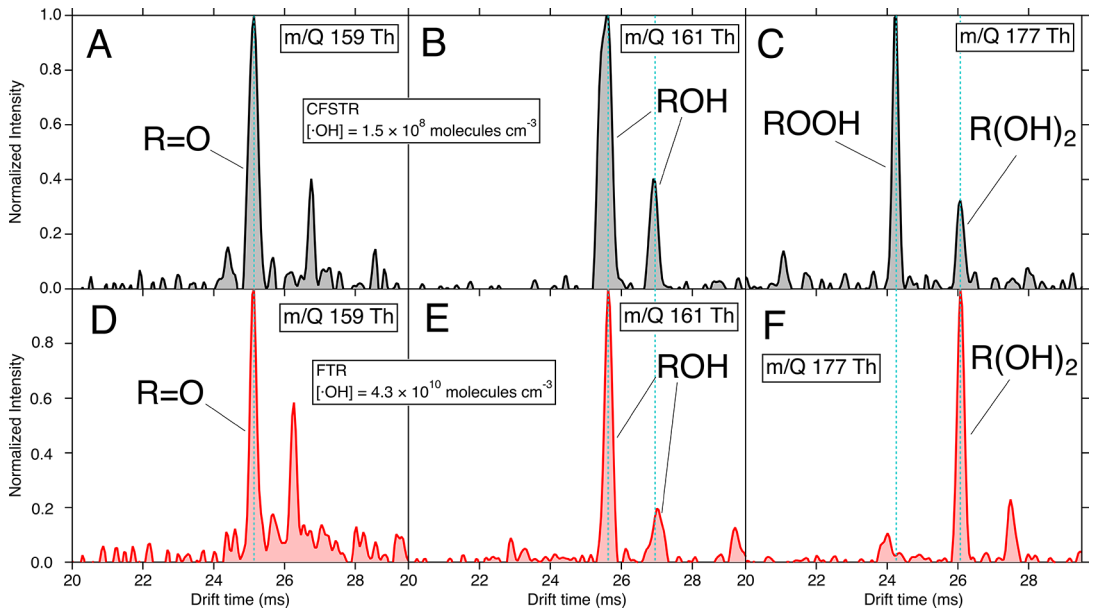

Figure 4. Comparison of R═O, ROH, and "RH + 2O" on the isomeric level between CFSTR (A−C) and FTR (D−F) experiments by the IMS-MS. The same drift time peaks suggest identical structures. The unique peak in (C) at 24.2 ms in m/Q 177 Th, specific only to the low-[•OH] CFSTR experiment, is identified as the ROOH.

test whether the ROOH formation is formed from the $RO_2^•$ + $HO_2^•$ reactions, we incorporated $HO_2^•$ uptake and subsequent $RO_2^•$ + $HO_2^•$ reactions into the model using known kinetic parameters.[47,48] However, the results suggest that this process

https://doi.org/10.1021/acs.est.2c09773
Environ. Sci. Technol. 2023, 57, 6965−6974

plays a negligible role in γ_{eff} prediction and is unlikely to produce sufficient ROOH under the studied conditions (see the Supporting Information). In support of this, [$^{\bullet}HO_2$] is expected to be higher with increased [$^{\bullet}OH$] and thus, ROOH formed from $RO_2^{\bullet}$ + $HO_2^{\bullet}$ should also increase with [$^{\bullet}OH$], which is opposite to the observed ROOH trend (Figure 3D). It should also be pointed out that during thermal desorption in TD-CIMS, decomposition of the products, especially ROOH, cannot be ruled out. However, thermal decomposition should not affect the ROOH trends shown in Figure 3 and may indicate that the formation of ROOH is even more important.

Autoxidation as the Key Aging Mechanism. Through relating the enhancement of both γ_{eff} and ROOH formation under low [$^{\bullet}OH$], we propose a chain reaction mechanism between $RO_2^{\bullet}$ and RH, leading to the formation of ROOH and regenerating $RO_2^{\bullet}$ in the presence of O_2 (Figure 2, bottom part). The formed ROOH may decompose into $RO^{\bullet}$ and $^{\bullet}OH$, both of which could abstract H from RH in the condensed phase. This $RO_2^{\bullet}$-mediated mechanism thus sustains the other chain reaction ($RO^{\bullet}$ + RH) and creates additional secondary pathways to consume RH and form ROH and $RO_2^{\bullet}$, further increasing γ_{eff}. Under high [$^{\bullet}OH$], the large $^{\bullet}OH$ flux at the particle surface leads to the substantial formation of $RO_2^{\bullet}$, thus favoring the $RO_2^{\bullet}$ + $RO_2^{\bullet}$ self-reaction. With lower [$^{\bullet}OH$], the interfacial and particle-phase [$RO_2^{\bullet}$] also decreases, allowing for the competing $RO_2^{\bullet}$ + RH reaction to become non-negligible. As a result, the formation of ROOH is promoted and that of R(=O) is inhibited with low [$^{\bullet}OH$]; in contrast, ROH may be formed in both processes. This mechanism has been known for decades in biochemistry and polymer chemistry for lipids and rubbers (also known as "autoxidation"),[49−51] but for the first time here, this mechanism is reported in aerosol chemistry. It should be noted that this intermolecular autoxidation mechanism is essentially different from the unimolecular autoxidation chemistry (i.e., intramolecular H-shift followed by O_2 addition) for gas-phase $RO_2^{\bullet}$.[52] Here, we demonstrate that the intermolecular autoxidation mechanism in the condensed phase exhibits a unique [$^{\bullet}OH$]-dependent behavior in aerosol chemistry, suggesting that the OA heterogeneous oxidation results obtained in the past decades may not accurately describe the processes occurring in the real atmosphere.

Following the proposal of the autoxidation mechanism, we implemented it into the kinetic model to aid the interpretation of the experimental results. The $RO_2^{\bullet}$ + RH reaction rate constant is estimated to be on the order of 10^{-6} times slower than that for $RO^{\bullet}$ + RH.[53] The ROOH decomposition rate may vary significantly, likely owing to the stability and reactivity of the ROOH. Although some studies showed that ROOH can be stable in room temperature for as long as 24 h,[54,55] ROOH in atmospheric OA were more often found to be rather labile, especially for the highly functionalized molecules, with the first-order decomposition rate ranging from 3×10^{-5} s^{-1} to $\sim 2 \times 10^{-3}$ s^{-1}.[56−59] Furthermore, little is known regarding the detailed ROOH decomposition mechanism and products. Unimolecular decomposition via breaking the weak O−O bond to form $RO^{\bullet}$ and $^{\bullet}OH$ was suggested as a possible reaction at ambient temperature for peroxides with O/C ratios at 0.5 or higher.[56] In addition, bimolecular reactions were also suggested, such as the Baeyer−Villiger reaction and Korcek mechanism.[57,60] However, these bimolecular mechanisms do not directly produce free radicals and hence cannot propagate the chain reactions shown in Figure 2. The lack of detailed kinetic and mechanistic understanding leads to great challenges to explicitly incorporate the ROOH chemistry into the kinetic model. Therefore, we lumped the possible ROOH unimolecular[56] and bimolecular[57] decomposition pathways as a single pseudo first-order decomposition reaction forming $RO^{\bullet}$ + $^{\bullet}OH$ with a first-order decomposition rate constant and a tunable yield (see the Supporting Information for model details).

Despite the simplification, this model reasonably reflects the chain propagating nature of the autoxidation mechanism. To capture the observed γ_{eff}−[$^{\bullet}OH$] relationship over the entire studied [$^{\bullet}OH$] range, optimization suggests that the model needs to constrain the formation rate of $RO^{\bullet}$ + $^{\bullet}OH$ from ROOH decomposition at 1×10^{-5}−1×10^{-4} s^{-1}, while keeping the $RO_2^{\bullet}$ + RH reaction rate constant in a reasonable range (i.e., 5−20 $\times 10^{-21}$ cm^3 $molecules^{-1}$ s^{-1}) for all the studied OA systems. Here, the formation rate of $RO^{\bullet}$ + $^{\bullet}OH$ is a combination of ROOH decomposition rate and the branching ratio of $RO^{\bullet}$ + $^{\bullet}OH$. For example, if all the ROOH decomposition forms $RO^{\bullet}$ + $^{\bullet}OH$, the decomposition rate is the same as the formation rate of $RO^{\bullet}$ + $^{\bullet}OH$, while if only 10% of ROOH decomposes to $RO^{\bullet}$ + $^{\bullet}OH$, the overall ROOH decomposition rate needs to be approximately 1 order of magnitude higher, which is still within the range of previously reported ROOH decomposition rate constant mentioned above.[56−59] Model simulations of the γ_{eff}−[$^{\bullet}OH$] relationship using the autoxidation mechanism agree nicely with the measurements (Figure 1), suggesting that autoxidation in the condensed phase can indeed greatly accelerate OA aging under atmospherically relevant [$^{\bullet}OH$]. It should be noted that the good model-observation agreement does not require a certain unique set of parameters. Rather, with a given formation rate of $RO^{\bullet}$ + $^{\bullet}OH$ in the above-mentioned range, a coupled $RO_2^{\bullet}$ + RH reaction rate constant can be determined to result in a similarly good agreement as shown in Figure 1. Furthermore, it is remarkable that the model results also agree with the trends of [$^{\bullet}OH$]-dependent fractions of R=O and "RH + 2O" (Figure 3C,D), further supporting the autoxidation mechanism. Lastly, to test whether other radical-involved chemical processes might affect or contribute to the enhanced OA degradation, unimolecular H-shift isomerization for $RO_2^{\bullet}$ and $RO^{\bullet}$ were considered in the kinetic model. This unimolecular process has been shown to play important roles in the gas phase,[52,61,62] but our model simulations suggest that they are not fast enough at typical reaction rate constants to compete with the autoxidation mechanism and play a very minor role in OA aging kinetics (see the Supporting Information).

The kinetic model further suggests that autoxidation-involved reactions (i.e., RH + $RO_2^{\bullet}$, RH + $RO^{\bullet}$, and RH + $^{\bullet}OH$ from ROOH decomposition) could account for >95% of total RH consumption under atmospheric [$^{\bullet}OH$] (Figure S9). This means that the collision of gas-phase $^{\bullet}OH$ with OA particles plays more of an initiator role, rather than acting as the dominant oxidant of OA under atmospheric conditions. This also implies that once the oxidation is triggered, autoxidation may proceed even in the dark. Since most of the OA molecules are not oxidized directly by the $^{\bullet}OH$ from gas-phase adsorption under low [$^{\bullet}OH$], the OA oxidation is no longer confined to the interfacial region of the particles. Consistently, model results suggest that the OA oxidation could occur throughout the entire particles under atmospherically relevant [$^{\bullet}OH$], contrary to the dominant interfacial

https://doi.org/10.1021/acs.est.2c09773
Environ. Sci. Technol. 2023, 57, 6965−6974

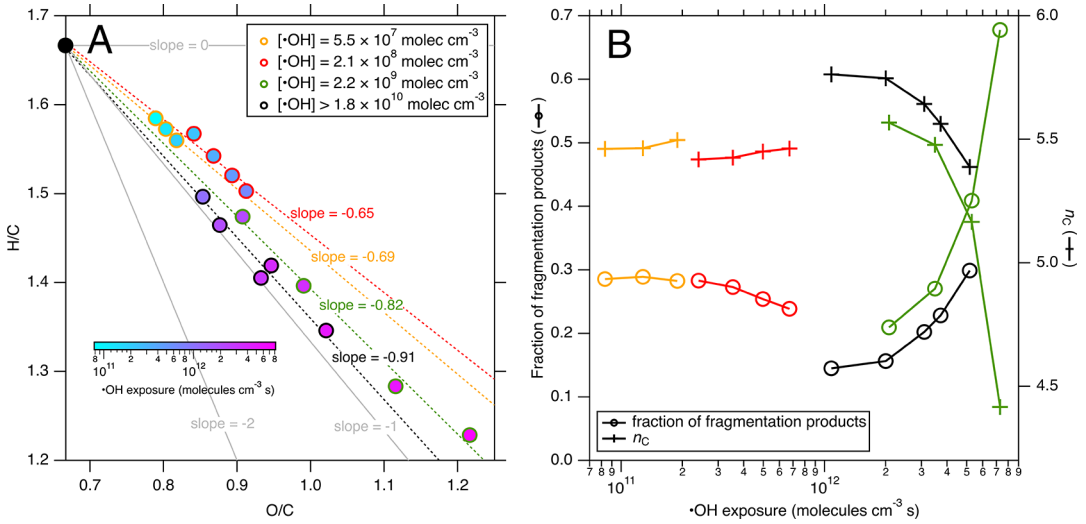

Figure 5. Chemical composition of oxidized 3-methylglutaric acid OA. (A) The Van Krevelen diagram for four 3-methylglutaric acid oxidation experiments. The experiment with the highest [•OH] was performed in the FTR and the other three lower-[•OH] experiments were performed in the CFSTR. The linear fits with slopes are shown with the data; the color scale indicates the •OH exposure for each data point. (B) The fraction of fragmentation products (left axis) and n_C (right axis) as a function of •OH exposure for the same 3-methylglutaric acid oxidation experiments as in (A).

oxidation under much higher [•OH] for all the examined OA systems (Figure S10). Thus, for particles that are viscous and do not rapidly mix, autoxidation could make a big difference. Beyond the D_{org} range for the studied OA, the simulations indicate that even for more viscous OA particle across the semisolid and solid ranges, the OA oxidation events could still spread throughout the particles in about an hour under atmospheric [•OH] (Figure S11). These simulations highlight that the autoxidation mechanism leads to highly efficient OA aging by allowing the oxidation to occur in the particle bulk and bypassing diffusion limitations, hence making the viscous particles more homogeneous during oxidation.

Overall Aerosol Composition Influenced by Autoxidation. Finally, we investigated how intermolecular autoxidation may impact the entire OA composition. For this purpose, we focus on the 3-methylglutaric acid system which is more readily oxidized and can form diverse oxidation products.[24] The observed oxidation products ($C_{1-6}H_{2-10}O_{3-8}$) by the IMS-MS were employed to calculate the intensity-based elemental ratios, averaged carbon number (n_C), and fraction of fragmentation products in the particle phase under different oxidation conditions (Figure 5). As the Van Krevelen diagram shown in Figure 5A, the FTR experiments with the highest [•OH] (>∼ 2×10^{10} molecules cm^{-3}) exhibit the steepest H/C−O/C trajectory, with a slope ∼ −0.91, indicative of a mechanism that forms similar amounts of carbonyls and alcohols (consistent with the Russell mechanism). In comparison, the lower [•OH] CFSTR experiments all had shallower H/C−O/C trajectories, with slopes of −0.65−−0.69 under [•OH] < ∼ 2×10^8 molecules cm^{-3} and −0.82 under [•OH] ∼ 2×10^9 molecules cm^{-3}. The slope shift as a function of [•OH] suggests that low [•OH] favors the formation of alcohols and hydroperoxides over carbonyls, consistent with the autoxidation mechanism. This mechanistic difference was also supported by comparing the major functionalization products: higher abundance of alcohols and hydroperoxides were observed in the CFSTR than the FTR (Figure S12) and higher ratios of the "RH + 2O" signals over the other two major second-generation products were found under lower [•OH] (Figure S13). As a result of the enhanced hydroperoxides by autoxidation, the low-[•OH] CFSTR experiments reached comparable carbon oxidation states with the high-[•OH] FTR experiments, but at much lower •OH exposure (Figure S14). It is also evident that under [•OH] > ∼ 2×10^9 molecules cm^{-3} (in both reactors), the fraction of fragmentation products increases and n_C decreases exponentially with •OH exposure (Figure 5B), consistent with prior understanding that fragmentation is increasingly important after the functionalization products are further oxidized. However, under lower [•OH] (<∼ 2×10^8 molecules cm^{-3}), an appreciable fraction of the total measured products are fragmentation products (20−30% based on peak intensities, Figure 5B), even with very low •OH exposure (i.e., < 10^{11} molecules cm^{-3} s). We suggest that this is because the enhanced autoxidation under low [•OH] promotes RO• formation through ROOH decomposition and hence increase fragmentation even with low •OH exposure. These results suggest that autoxidation could provide a new pathway to rapidly produce small, oxidized compounds which could evaporate to the gas phase and contribute to important atmospheric processes such as secondary OA formation.

Overall, the chemical composition of oxidized OA provides observation-based support to the autoxidation mechanism and ROOH decomposition pathways. Specifically, the increased formation of alcohol and fragmentation products under lower [•OH] strongly supports the ROOH unimolecular decomposition to RO• + •OH;[56] the enhanced alcohol formation may also be partly due to the Baeyer−Villiger reactions.[60] Therefore, it is likely that both ROOH processes take place to promote autoxidation and explain the measurements.

■ ATMOSPHERIC IMPLICATIONS

In this work, we report strong and direct evidence for an intermolecular autoxidation mechanism in heterogeneous oxidative aging of OA. Although only a few highly oxidized OA surrogates were examined, its chemical nature is rather nonspecific.[50,51,53] Previous work showed a somewhat similar γ_{eff}−[•OH] dependence, but to a lesser degree for less oxidized

https://doi.org/10.1021/acs.est.2c09773
Environ. Sci. Technol. 2023, 57, 6965−6974

OA surrogates.[7,19,63] This could be caused by different kinetic parameters in the autoxidation mechanism (Figure S15). We show that autoxidation may occur at much faster rates than the other particle-phase $RO_2^•$ pathways under atmospherically relevant [$^•OH$] (e.g., $RO_2^•$ reactions with $RO_2^•$ and $HO_2^•$) and significantly boost OA oxidation. Through autoxidation, OA oxidative aging in the atmosphere may proceed on timescales from less than a day to several days, much more rapidly than prior laboratory results have suggested. This result opens up new avenues for heterogeneous OA oxidation to play key roles in various atmospheric processes. Although the laboratory studies showed clear evidence for enhanced OA aging kinetics and the formation of ROOH, ROH, and fragmentation products, the autoxidation-involved kinetic parameters have large uncertainties. This is mainly caused by (1) the RH + $RO_2^•$ reaction kinetics have been less studied for system relevant to atmospheric OA species;[53] and (2) the ROOH decomposition rate constant and mechanism are largely varied with chemical structures.[56−59] Therefore, the corresponding kinetic model is constrained within the wide ranges of reported values to the best of our knowledge. Thus, future studies are needed to help better determine the key parameters for more accurate prediction of multiphase OA aging kinetics.

In the atmosphere, many OA processes could occur simultaneous with aging (e.g., secondary aerosol formation, new particle formation and growth, aqueous-phase reactions, evaporation, and so forth); thus, direct field evidence to support such rapid OA oxidation is unavailable. However, the autoxidation-mediated fast OA aging reported in this work should be considered in the interpretation of field measurements. Another surprising outcome of our findings is that the gas-phase $^•OH$ is only an initiator of OA aging, rather than the main oxidant, implying that OA oxidative aging may efficiently take place even under dark conditions (e.g., nighttime or in indoor environments). Additionally, substantial ROOH may be present in the oxidized OA particles as reactive oxygen species, which are well known to result in health effects.[64] We also suggest that autoxidation can lead to OA oxidation throughout the entire aerosol particle even for highly viscous OA, rather than confined at the gas-particle interface, as previously understood. Lastly, we show that autoxidation may have an extending influence on the entire OA particle composition during oxidative aging. It will increase the oxygenation of OA efficiently and facilitate fragmentation chemistry. The rapid and enhanced oxygenation of aerosol particles through this mechanism may result in increased cloud formation, leading to larger indirect climate effects. Overall, the autoxidation mechanism reported here unveils the nature of heterogeneous aerosol oxidation chemistry and highlights the need to rethink aerosol aging processes in the real atmosphere.

■ ASSOCIATED CONTENT

Supporting Information

The Supporting Information is available free of charge at https://pubs.acs.org/doi/10.1021/acs.est.2c09773.

Additional experimental details of reactor schematics, OA and VOC decay data, mass spectral data, and peroxide measurements, the multilayer reaction-diffusion kinetic model simulations and sensitivity analysis (PDF)

■ AUTHOR INFORMATION

Corresponding Author

Haofei Zhang − *Department of Chemistry, University of California, Riverside, California 92507, United States;* orcid.org/0000-0002-7936-4493; Email: haofei.zhang@ucr.edu

Authors

Wen Zhang − *Department of Chemistry, University of California, Riverside, California 92507, United States*

Zixu Zhao − *Department of Chemistry, University of California, Riverside, California 92507, United States;* Present Address: Department of Environmental Sciences, Policy, and Management, University of California, Berkeley, California 94720, USA

Chuanyang Shen − *Department of Chemistry, University of California, Riverside, California 92507, United States*

Complete contact information is available at: https://pubs.acs.org/10.1021/acs.est.2c09773

Notes

The authors declare no competing financial interest.

■ ACKNOWLEDGMENTS

This work was supported by the U.S. National Science Foundation (CHE-2002413).

■ REFERENCES

(1) Zhang, Q.; Jimenez, J. L.; Canagaratna, M. R.; Allan, J. D.; Coe, H.; Ulbrich, I.; Alfarra, M. R.; Takami, A.; Middlebrook, A. M.; Sun, Y. L.; Dzepina, K.; Dunlea, E.; Docherty, K.; DeCarlo, P. F.; Salcedo, D.; Onasch, T.; Jayne, J. T.; Miyoshi, T.; Shimono, A.; Hatakeyama, S.; Takegawa, N.; Kondo, Y.; Schneider, J.; Drewnick, F.; Borrmann, S.; Weimer, S.; Demerjian, K.; Williams, P.; Bower, K.; Bahreini, R.; Cottrell, L.; Griffin, R. J.; Rautiainen, J.; Sun, J. Y.; Zhang, Y. M.; Worsnop, D. R. Ubiquity and dominance of oxygenated species in organic aerosols in anthropogenically-influenced Northern Hemisphere midlatitudes. *Geophys. Res. Lett.* **2007**, *34*, L13801.

(2) Jimenez, J. L.; Canagaratna, M. R.; Donahue, N. M.; Prevot, A. S. H.; Zhang, Q.; Kroll, J. H.; DeCarlo, P. F.; Allan, J. D.; Coe, H.; Ng, N. L.; Aiken, A. C.; Docherty, K. S.; Ulbrich, I. M.; Grieshop, A. P.; Robinson, A. L.; Duplissy, J.; Smith, J. D.; Wilson, K. R.; Lanz, V. A.; Hueglin, C.; Sun, Y. L.; Tian, J.; Laaksonen, A.; Raatikainen, T.; Rautiainen, J.; Vaattovaara, P.; Ehn, M.; Kulmala, M.; Tomlinson, J. M.; Collins, D. R.; Cubison, M. J.; Dunlea, J.; Huffman, J. A.; Onasch, T. B.; Alfarra, M. R.; Williams, P. I.; Bower, K.; Kondo, Y.; Schneider, J.; Drewnick, F.; Borrmann, S.; Weimer, S.; Demerjian, K.; Salcedo, D.; Cottrell, L.; Griffin, R.; Takami, A.; Miyoshi, T.; Hatakeyama, S.; Shimono, A.; Sun, J. Y.; Zhang, Y. M.; Dzepina, K.; Kimmel, J. R.; Sueper, D.; Jayne, J. T.; Herndon, S. C.; Trimborn, A. M.; Williams, L. R.; Wood, E. C.; Middlebrook, A. M.; Kolb, C. E.; Baltensperger, U.; Worsnop, D. R.; et al. Evolution of Organic Aerosols in the Atmosphere. *Science* **2009**, *326*, 1525−1529.

(3) Boucher, O.; Randall, D.; Artaxo, P.; Bretherton, C.; Feingold, C.; Forster, P.; Kerminen, V.-M.; Kondo, Y.; Liao, H.; Lohmann, U.; Rasch, P.; Satheesh, S. K.; Sherwood, S.; Stevens, B.; Zhang, X.-Y. *Clouds and Aerosols*; IPCC, 2013, p 657.

(4) Dockery, D. W.; Pope, C. A.; Xu, X.; Spengler, J. D.; Ware, J. H.; Fay, M. E.; Ferris, B. G.; Speizer, F. E. An Association between Air Pollution and Mortality in Six U.S. Cities. *N. Engl. J. Med.* **1993**, *329*, 1753−1759.

(5) George, I. J.; Abbatt, J. P. D. Heterogeneous oxidation of atmospheric aerosol particles by gas-phase radicals. *Nat. Chem.* **2010**, *2*, 713−722.

(6) George, I. J.; Vlasenko, A.; Slowik, J. G.; Broekhuizen, K.; Abbatt, J. P. D. Heterogeneous oxidation of saturated organic aerosols

by hydroxyl radicals: uptake kinetics, condensed-phase products, and particle size change. *Atmos. Chem. Phys.* **2007**, *7*, 4187−4201.
(7) Smith, J. D.; Kroll, J. H.; Cappa, C. D.; Che, D. L.; Liu, C. L.; Ahmed, M.; Leone, S. R.; Worsnop, D. R.; Wilson, K. R. The heterogeneous reaction of hydroxyl radicals with sub-micron squalane particles: a model system for understanding the oxidative aging of ambient aerosols. *Atmos. Chem. Phys.* **2009**, *9*, 3209−3222.
(8) George, I. J.; Abbatt, J. P. D. Chemical evolution of secondary organic aerosol from OH-initiated heterogeneous oxidation. *Atmos. Chem. Phys.* **2010**, *10*, 5551−5563.
(9) Kroll, J. H.; Lim, C. Y.; Kessler, S. H.; Wilson, K. R. Heterogeneous Oxidation of Atmospheric Organic Aerosol: Kinetics of Changes to the Amount and Oxidation State of Particle-Phase Organic Carbon. *J. Phys. Chem. A* **2015**, *119*, 10767−10783.
(10) Kessler, S. H.; Nah, T.; Daumit, K. E.; Smith, J. D.; Leone, S. R.; Kolb, C. E.; Worsnop, D. R.; Wilson, K. R.; Kroll, J. H. OH-Initiated Heterogeneous Aging of Highly Oxidized Organic Aerosol. *J. Phys. Chem. A* **2012**, *116*, 6358−6365.
(11) Davies, J. F.; Wilson, K. R. Nanoscale interfacial gradients formed by the reactive uptake of OH radicals onto viscous aerosol surfaces. *Chem. Sci.* **2015**, *6*, 7020−7027.
(12) Hearn, J. D.; Renbaum, L. H.; Wang, X.; Smith, G. D. Kinetics and products from reaction of Cl radicals with dioctyl sebacate (DOS) particles in O2: a model for radical-initiated oxidation of organic aerosols. *Phys. Chem. Chem. Phys.* **2007**, *9*, 4803−4813.
(13) Chan, M. N.; Zhang, H.; Goldstein, A. H.; Wilson, K. R. Role of Water and Phase in the Heterogeneous Oxidation of Solid and Aqueous Succinic Acid Aerosol by Hydroxyl Radicals. *J. Phys. Chem. C* **2014**, *118*, 28978−28992.
(14) Arangio, A. M.; Slade, J. H.; Berkemeier, T.; Pöschl, U.; Knopf, D. A.; Shiraiwa, M. Multiphase Chemical Kinetics of OH Radical Uptake by Molecular Organic Markers of Biomass Burning Aerosols: Humidity and Temperature Dependence, Surface Reaction, and Bulk Diffusion. *J. Phys. Chem. A* **2015**, *119*, 4533−4544.
(15) Slade, J. H.; Knopf, D. A. Heterogeneous OH oxidation of biomass burning organic aerosol surrogate compounds: assessment of volatilisation products and the role of OH concentration on the reactive uptake kinetics. *Phys. Chem. Chem. Phys.* **2013**, *15*, 5898−5915.
(16) Kristiansen, N. I.; Stohl, A.; Olivié, D. J. L.; Croft, B.; Søvde, O. A.; Klein, H.; Christoudias, T.; Kunkel, D.; Leadbetter, S. J.; Lee, Y. H.; Zhang, K.; Tsigaridis, K.; Bergman, T.; Evangeliou, N.; Wang, H.; Ma, P. L.; Easter, R. C.; Rasch, P. J.; Liu, X.; Pitari, G.; Di Genova, G.; Zhao, S. Y.; Balkanski, Y.; Bauer, S. E.; Faluvegi, G. S.; Kokkola, H.; Martin, R. V.; Pierce, J. R.; Schulz, M.; Shindell, D.; Tost, H.; Zhang, H. Evaluation of observed and modelled aerosol lifetimes using radioactive tracers of opportunity and an ensemble of 19 global models. *Atmos. Chem. Phys.* **2016**, *16*, 3525−3561.
(17) Zhang, H.; Ruehl, C. R.; Chan, A. W. H.; Nah, T.; Worton, D. R.; Isaacman, G.; Goldstein, A. H.; Wilson, K. R. OH-initiated heterogeneous oxidation of cholestane: A model system for understanding the photochemical aging of cyclic alkane aerosols. *J. Phys. Chem. A* **2013**, *117*, 12449−12458.
(18) Renbaum, L. H.; Smith, G. D. Artifacts in measuring aerosol uptake kinetics: the roles of time, concentration and adsorption. *Atmos. Chem. Phys.* **2011**, *11*, 6881−6893.
(19) Richards-Henderson, N. K.; Goldstein, A. H.; Wilson, K. R. Large Enhancement in the Heterogeneous Oxidation Rate of Organic Aerosols by Hydroxyl Radicals in the Presence of Nitric Oxide. *J. Phys. Chem. Lett.* **2015**, *6*, 4451−4455.
(20) Chim, M. M.; Lim, C. Y.; Kroll, J. H.; Chan, M. N. Evolution in the Reactivity of Citric Acid toward Heterogeneous Oxidation by Gas-Phase OH Radicals. *ACS Earth Space Chem.* **2018**, *2*, 1323−1329.
(21) Che, D. L.; Smith, J. D.; Leone, S. R.; Ahmed, M.; Wilson, K. R. Quantifying the reactive uptake of OH by organic aerosols in a continuous flow stirred tank reactor. *PCCP, Phys. chem. chem. phys. (Print)* **2009**, *11*, 7885−7895.
(22) Richards-Henderson, N. K.; Goldstein, A. H.; Wilson, K. R. Sulfur Dioxide Accelerates the Heterogeneous Oxidation Rate of Organic Aerosol by Hydroxyl Radicals. *Environ. Sci. Technol.* **2016**, *50*, 3554−3561.
(23) Zeng, M.; Heine, N.; Wilson, K. R. Evidence that Criegee intermediates drive autoxidation in unsaturated lipids. *Proc. Natl. Acad. Sci. U. S. A.* **2020**, *117*, 4486−4490.
(24) Zhao, Z.; Yang, X.; Lee, J.; Tolentino, R.; Mayorga, R.; Zhang, W.; Zhang, H. Diverse Reactions in Highly Functionalized Organic Aerosols during Thermal Desorption. *ACS Earth Space Chem.* **2020**, *4*, 283−296.
(25) Virtanen, A.; Joutsensaari, J.; Koop, T.; Kannosto, J.; Yli-Pirilä, P.; Leskinen, J.; Mäkelä, J. M.; Holopainen, J. K.; Pöschl, U.; Kulmala, M.; Worsnop, D. R.; Laaksonen, A. An amorphous solid state of biogenic secondary organic aerosol particles. *Nature* **2010**, *467*, 824−827.
(26) Shiraiwa, M.; Li, Y.; Tsimpidi, A. P.; Karydis, V. A.; Berkemeier, T.; Pandis, S. N.; Lelieveld, J.; Koop, T.; Pöschl, U. Global distribution of particle phase state in atmospheric secondary organic aerosols. *Nat. Commun.* **2017**, *8*, 15002.
(27) Zhao, Z.; Tolentino, R.; Lee, J.; Vuong, A.; Yang, X.; Zhang, H. Interfacial Dimerization by Organic Radical Reactions during Heterogeneous Oxidative Aging of Oxygenated Organic Aerosols. *J. Phys. Chem. A* **2019**, *123*, 10782−10792.
(28) Zhao, Z.; Xu, Q.; Yang, X.; Zhang, H. Heterogeneous Ozonolysis of Endocyclic Unsaturated Organic Aerosol Proxies: Implications for Criegee Intermediate Dynamics and Later-Generation Reactions. *ACS Earth Space Chem.* **2019**, *3*, 344−356.
(29) Zhao, Z.; Le, C.; Xu, Q.; Peng, W.; Jiang, H.; Lin, Y.-H.; Cocker, D. R.; Zhang, H. Compositional Evolution of Secondary Organic Aerosol as Temperature and Relative Humidity Cycle in Atmospherically Relevant Ranges. *ACS Earth Space Chem.* **2019**, *3*, 2549−2558.
(30) Zhao, Z.; Mayorga, R.; Lee, J.; Yang, X.; Tolentino, R.; Zhang, W.; Vuong, A.; Zhang, H. Site-Specific Mechanisms in OH-Initiated Organic Aerosol Heterogeneous Oxidation Revealed by Isomer-Resolved Molecular Characterization. *ACS Earth Space Chem.* **2020**, *4*, 783−794.
(31) Zhao, Z.; Zhang, W.; Alexander, T.; Zhang, X.; Martin, D. B. C.; Zhang, H. Isolating α-Pinene Ozonolysis Pathways Reveals New Insights into Peroxy Radical Chemistry and Secondary Organic Aerosol Formation. *Environ. Sci. Technol.* **2021**, *55*, 6700−6709.
(32) Mayorga, R. J.; Zhao, Z.; Zhang, H. Formation of secondary organic aerosol from nitrate radical oxidation of phenolic VOCs: Implications for nitration mechanisms and brown carbon formation. *Atmos. Environ.* **2021**, *244*, 117910.
(33) Price, H. C.; Murray, B. J.; Mattsson, J.; O'Sullivan, D.; Wilson, T. W.; Baustian, K. J.; Benning, L. G. Quantifying water diffusion in high-viscosity and glassy aqueous solutions using a Raman isotope tracer method. *Atmos. Chem. Phys.* **2014**, *14*, 3817−3830.
(34) Song, Y. C.; Haddrell, A. E.; Bzdek, B. R.; Reid, J. P.; Bannan, T.; Topping, D. O.; Percival, C.; Cai, C. Measurements and Predictions of Binary Component Aerosol Particle Viscosity. *J. Phys. Chem. A* **2016**, *120*, 8123−8137.
(35) Yuan, B.; Koss, A. R.; Warneke, C.; Coggon, M.; Sekimoto, K.; de Gouw, J. A. Proton-Transfer-Reaction Mass Spectrometry: Applications in Atmospheric Sciences. *Chem. Rev.* **2017**, *117*, 13187−13229.
(36) Zhang, X.; Krechmer, J. E.; Groessl, M.; Xu, W.; Graf, S.; Cubison, M.; Jayne, J. T.; Jimenez, J. L.; Worsnop, D. R.; Canagaratna, M. R. A novel framework for molecular characterization of atmospherically relevant organic compounds based on collision cross section and mass-to-charge ratio. *Atmos. Chem. Phys.* **2016**, *16*, 12945−12959.
(37) Krechmer, J. E.; Groessl, M.; Zhang, X.; Junninen, H.; Massoli, P.; Lambe, A. T.; Kimmel, J. R.; Cubison, M. J.; Graf, S.; Lin, Y. H.; Budisulistiorini, S. H.; Zhang, H.; Surratt, J. D.; Knochenmuss, R.; Jayne, J. T.; Worsnop, D. R.; Jimenez, J. L.; Canagaratna, M. R. Ion mobility spectrometry−mass spectrometry (IMS−MS) for on- and offline analysis of atmospheric gas and aerosol species. *Atmos. Meas. Tech.* **2016**, *9*, 3245−3262.

https://doi.org/10.1021/acs.est.2c09773
Environ. Sci. Technol. 2023, 57, 6965−6974

(38) Butkovskaya, N. I.; Kukui, A.; Pouvesle, N.; Le Bras, G. Rate Constant and Mechanism of the Reaction of OH Radicals with Acetic Acid in the Temperature Range of 229−300 K. *J. Phys. Chem. A* **2004**, *108*, 7021−7026.
(39) Singleton, D. L.; Paraskevopoulos, G.; Irwin, R. S. Rates and mechanism of the reactions of hydroxyl radicals with acetic, deuterated acetic, and propionic acids in the gas phase. *J. Am. Chem. Soc.* **1989**, *111*, 5248−5251.
(40) Houle, F. A.; Hinsberg, W. D.; Wilson, K. R. Oxidation of a model alkane aerosol by OH radical: the emergent nature of reactive uptake. *Phys. Chem. Chem. Phys.* **2015**, *17*, 4412−4423.
(41) Shiraiwa, M.; Pfrang, C.; Koop, T.; Pöschl, U. Kinetic multi-layer model of gas-particle interactions in aerosols and clouds (KM-GAP): linking condensation, evaporation and chemical reactions of organics, oxidants and water. *Atmos. Chem. Phys.* **2012**, *12*, 2777−2794.
(42) Wiegel, A. A.; Liu, M. J.; Hinsberg, W. D.; Wilson, K. R.; Houle, F. A. Diffusive confinement of free radical intermediates in the OH radical oxidation of semisolid aerosols. *Phys. Chem. Chem. Phys.* **2017**, *19*, 6814−6830.
(43) Slade, J. H.; Knopf, D. A. Multiphase OH oxidation kinetics of organic aerosol: The role of particle phase state and relative humidity. *Geophys. Res. Lett.* **2014**, *41*, 5297−5306.
(44) Houle, F. A.; Wiegel, A. A.; Wilson, K. R. Changes in Reactivity as Chemistry Becomes Confined to an Interface. The Case of Free Radical Oxidation of C30H62 Alkane by OH. *J. Phys. Chem. Lett.* **2018**, *9*, 1053−1057.
(45) Russell, G. A. Deuterium-isotope Effects in the Autoxidation of Aralkyl Hydrocarbons. Mechanism of the Interaction of PEroxy Radicals1. *J. Am. Chem. Soc.* **1957**, *79*, 3871−3877.
(46) McNeill, V. F.; Yatavelli, R. L. N.; Thornton, J. A.; Stipe, C. B.; Landgrebe, O. Heterogeneous OH oxidation of palmitic acid in single component and internally mixed aerosol particles: vaporization and the role of particle phase. *Atmos. Chem. Phys.* **2008**, *8*, 5465−5476.
(47) Lakey, P. S. J.; George, I. J.; Whalley, L. K.; Baeza-Romero, M. T.; Heard, D. E. Measurements of the HO2 Uptake Coefficients onto Single Component Organic Aerosols. *Environ. Sci. Technol.* **2015**, *49*, 4878−4885.
(48) Liu, M. J.; Wiegel, A. A.; Wilson, K. R.; Houle, F. A. Aerosol Fragmentation Driven by Coupling of Acid−Base and Free-Radical Chemistry in the Heterogeneous Oxidation of Aqueous Citric Acid by OH Radicals. *J. Phys. Chem. A* **2017**, *121*, 5856−5870.
(49) Smith, L. M.; Aitken, H. M.; Coote, M. L. The Fate of the Peroxyl Radical in Autoxidation: How Does Polymer Degradation Really Occur? *Acc. Chem. Res.* **2018**, *51*, 2006−2013.
(50) Foret, M. K.; Lincoln, R.; Do Carmo, S.; Cuello, A. C.; Cosa, G. Connecting the "Dots": From Free Radical Lipid Autoxidation to Cell Pathology and Disease. *Chem. Rev.* **2020**, *120*, 12757−12787.
(51) Helberg, J.; Pratt, D. A. Autoxidation vs. antioxidants − the fight for forever. *Chem. Soc. Rev.* **2021**, *50*, 7343−7358.
(52) Ehn, M.; Thornton, J. A.; Kleist, E.; Sipila, M.; Junninen, H.; Pullinen, I.; Springer, M.; Rubach, F.; Tillmann, R.; Lee, B.; Lopez-Hilfiker, F.; Andres, S.; Acir, I.-H.; Rissanen, M.; Jokinen, T.; Schobesberger, S.; Kangasluoma, J.; Kontkanen, J.; Nieminen, T.; Kurten, T.; Nielsen, L. B.; Jorgensen, S.; Kjaergaard, H. G.; Canagaratna, M.; Maso, M. D.; Berndt, T.; Petaja, T.; Wahner, A.; Kerminen, V.-M.; Kulmala, M.; Worsnop, D. R.; Wildt, J.; Mentel, T. F. A large source of low-volatility secondary organic aerosol. *Nature* **2014**, *506*, 476−479.
(53) Denisov, E. T.; Afanas'ev, I. B., *Oxidation and Antioxidants in Organic Chemistry and Biology*. Taylor & Francis: Boca Raton, FL, 2005, p 981
(54) Bakker-Arkema, J. G.; Ziemann, P. J. Measurements of Kinetics and Equilibria for the Condensed Phase Reactions of Hydroperoxides with Carbonyls to Form Peroxyhemiacetals. *ACS Earth Space Chem.* **2020**, *4*, 467−475.
(55) Maben, H. K.; Ziemann, P. J. Kinetics of oligomer-forming reactions involving the major functional groups present in atmospheric secondary organic aerosol particles. *Environmental Science: Processes & Impacts* **2023**, *25*, 214−228.
(56) Krapf, M.; El Haddad, I.; Bruns, E. A.; Molteni, U.; Daellenbach, K. R.; Prévôt, A. S. H.; Baltensperger, U.; Dommen, J. Labile Peroxides in Secondary Organic Aerosol. *Chem* **2016**, *1*, 603−616.
(57) Pospisilova, V.; Lopez-Hilfiker, F. D.; Bell, D. M.; El Haddad, I.; Mohr, C.; Huang, W.; Heikkinen, L.; Xiao, M.; Dommen, J.; Prevot, A. S. H.; Baltensperger, U.; Slowik, J. G. On the fate of oxygenated organic molecules in atmospheric aerosol particles. *Sci. Adv.* **2020**, *6*, No. eaax8922.
(58) Mertes, P.; Pfaffenberger, L.; Dommen, J.; Kalberer, M.; Baltensperger, U. Development of a sensitive long path absorption photometer to quantify peroxides in aerosol particles (Peroxide-LOPAP). *Atmos. Meas. Tech.* **2012**, *5*, 2339−2348.
(59) Pagonis, D.; Ziemann, P. J. Chemistry of hydroperoxycarbonyls in secondary organic aerosol. *Aerosol Sci. Technol.* **2018**, *52*, 1178−1193.
(60) Claflin, M. S.; Krechmer, J. E.; Hu, W.; Jimenez, J. L.; Ziemann, P. J. Functional Group Composition of Secondary Organic Aerosol Formed from Ozonolysis of α-Pinene Under High VOC and Autoxidation Conditions. *ACS Earth Space Chem.* **2018**, *2*, 1196−1210.
(61) Crounse, J. D.; Nielsen, L. B.; Jørgensen, S.; Kjaergaard, H. G.; Wennberg, P. O. Autoxidation of organic compounds in the atmosphere. *J. Phys. Chem. Lett.* **2013**, *4*, 3513−3520.
(62) Atkinson, R. Atmospheric reactions of alkoxy and β-hydroxyalkoxy radicals. *Int. J. Chem. Kinet.* **1997**, *29*, 99−111.
(63) Che, D. L.; Smith, J. D.; Leone, S. R.; Ahmed, M.; Wilson, K. R. Quantifying the reactive uptake of OH by organic aerosols in a continuous flow stirred tank reactor. *Phys. Chem. Chem. Phys.* **2009**, *11*, 7885−7895.
(64) Pöschl, U.; Shiraiwa, M. Multiphase Chemistry at the Atmosphere−Biosphere Interface Influencing Climate and Public Health in the Anthropocene. *Chem. Rev.* **2015**, *115*, 4440−4475.

https://doi.org/10.1021/acs.est.2c09773
Environ. Sci. Technol. 2023, 57, 6965−6974